

Room-temperature generation of giant pure spin currents using Co_2FeSi spin injectors

Takashi Kimura,^{1,2,*} Naoki Hashimoto,³
Shinya Yamada,³ Masanobu Miyao,^{3,2} and Kohei Hamaya^{3,4,†}

¹*Advanced Electronics Research Division,
INAMORI Frontier Research Center, Kyushu University,
744 Motooka, Fukuoka, 819-0395, Japan*

²*CREST, Japan Science and Technology Agency,
Sanbancho, Tokyo 102-0075, Japan*

³*Department of Electronics, Kyushu University,
744 Motooka, Fukuoka 819-0395, Japan*

⁴*PRESTO, Japan Science and Technology Agency,
Sanbancho, Tokyo 102-0075, Japan*

(Dated: November 10, 2018)

*kimura@ifrc.kyushu-u.ac.jp

†hamaya@ed.kyushu-u.ac.jp

Generation, manipulation, and detection of a pure spin current, i.e., the flow of spin angular momentum without a charge current[1–6], are prospective approaches for realizing next-generation spintronic devices with ultra low electric power consumptions. Conventional ferromagnetic electrodes such as Co and NiFe have so far been utilized as a spin injector for generating the pure spin currents in nonmagnetic channels[1, 2, 6–14]. However, the generation efficiency of the pure spin currents is extremely low at room temperature, giving rise to a serious obstacle for device applications. Here, we demonstrate the generation of giant pure spin currents at room temperature in lateral spin valve devices with a highly ordered Heusler-compound Co_2FeSi spin injector. The generation efficiency of the pure spin currents for the Co_2FeSi spin injectors reaches approximately one hundred times as large as that for NiFe ones, indicating that Heusler-compound spin injectors enable us to materialize a high-performance lateral spin device. The present study is a technological jump in spintronics and indicates the great potential of ferromagnetic Heusler compounds with half metallicity for generating pure spin currents.

Electrical spin injection from a ferromagnet (F) into a nonmagnet (N) can generate a spin current, i.e., the flow of spin angular momentum, even in a nonmagnetic channel[15]. In general, the spin current is induced by diffusing non-equilibrium spin accumulations in the vicinity of the F/N interface under the spin injection. However, since the difference in the density of states between majority and minority spins, i.e., spin polarization P , is not so large for a conventional F such as Co or NiFe (Py), the induced spin current in the N mainly returns back to the F (Fig. 1a). This gives rise to an extremely low injection efficiency of the spin current in the N[6, 16, 17]. If we utilize a perfectly spin-polarized F, so called a half-metallic ferromagnet (HMF)[18], as a spin injector, fully spin-polarized electrons can be injected into the N and the backflow of the spin currents can be completely suppressed, resulting in a dramatical improvement of the injection efficiency of the spin currents in the N (Fig. 1b). Also, one can extract a charge current by using nonlocal electrical spin injection in a mesoscopic lateral geometry, and can transfer only a spin current without the charge current, i.e., a pure spin current (Fig. 1c), in the nonmagnetic channel. In this scheme, using HMF spin injectors is a key for generating a *giant* pure spin current in the N (Fig. 1d).

As materials with half metallicity, we focus on Co-based Heusler compounds which enable huge tunnel magnetoresistance (TMR) and giant magnetoresistance (GMR) effects in vertical stacking device structures[19–21]. Despite these high performances, none of the lateral spin transports using the Heusler-compound electrodes have been reported yet. Thus, the combination of the high-performance Co-based Heusler compounds with laterally configured device structures is a prospective challenge for highly efficient generation of the pure spin currents. In this work, we show that a Co-based Heusler compound, Co_2FeSi (CFS), enables the highly efficient injection of the spin currents.

Our device structure is a lateral spin valve (LSV) consisting of the CFS spin injector and detector bridged by a Cu strip (Fig. 2a), where the CFS thin film with highly ordered $L2_1$ structures has been epitaxially grown on Si(111)[22]. Details of the growth of the CFS thin films and the fabrication processes of the LSVs are given in the Methods sections. As shown in Fig. 2b, a pure spin current generated by the nonlocal spin injection from CFS1 can be detected by CFS2 after the propagation of 600-nm distance in the Cu strip. Figure 2c shows a nonlocal magnetoresistance of the CFS/Cu LSV measured at room temperature (RT), together with that of a Py/Cu LSV. Here, the size of the CFS/Cu junction is three times as large as that of the Py/Cu junction. Note that a giant spin signal (ΔR_S) of 2.3

$m\Omega$ is seen for the CFS/Cu LSV (Fig. 2c), which is approximately ten times as large as that for the Py/Cu LSV. Since the spin injection efficiency is inversely proportional to the size of the F/N junctions [6], the giant ΔR_S demonstrated in the CFS/Cu LSV with larger sizes in the junctions implies a great possibility of the present CFS/Cu LSV. We also show the local spin valve signal of 4.5 m Ω at RT for the same CFS/Cu LSV (Fig. 2d). The value of 4.5 m Ω is almost twice of the non-local ΔR_S , in reasonable agreement with the previous reports [2, 6]. This means that one dimensional spin diffusion model well describes the spin transport in the present CFS/Cu LSV. Figure 2e shows a dependence of ΔR_S on the bias current density (J_{inj}) at the injecting junction for the CFS/Cu LSV, which is almost same as that for the Py/Cu LSV. The reduction of the ΔR_S is less than 20 % even under a high bias current density ($\sim 10^{11}$ A/m²), indicating much superior property compared to the LSV consisting of the high resistive tunnel junctions, where the ΔR_S drastically decreases even at low bias current density ($\sim 10^8$ A/m²)[11]. The temperature dependence of ΔR_S for the CFS/Cu LSV is also almost same as that for the Py/Cu LSV, where the ΔR_S takes a maximum value around 20 K, below which the ΔR_S decreases with decreasing temperature (Fig. 2f). This behavior can be explained by an enhancement in the spin-flip scattering at the Cu surface for the CFS/Cu LSV below 20 K, as discussed in Ref [10]. Surprisingly, the ΔR_S for the CFS/Cu exceeds 10 m Ω below 70 K (inset of Fig. 2f). From these results, we recognize that the present CFS/Cu LSV can be treated as conventional ohmic LSVs and can generate a giant pure spin current with a much less electric power than previously reported LSVs[1, 2, 6–14].

To quantitatively evaluate the device performance of the present LSVs from the nonlocal spin signals, we measured ΔR_S of CFS/Cu LSV devices with various distances (d), together with Py/Cu LSV devices as references, where d is the centre-centre distance between spin injector and detector. Here, we introduce a characteristic value in the LSV devices by extending the resistance change area product, commonly utilized to characterize the device performances in the vertical spin devices[24, 25]. The resistance change area product for the nonlocal spin signal, i.e., $\Delta R_S A$, is defined as $\Delta R_S (S_{inj} S_{det} / S_N)$, where S_{inj} , S_{det} , and S_N are the junction sizes in the spin injector and detector, and the cross section of the nonmagnetic strip. This $\Delta R_S A$ allows us to equivalently compare the generation efficiency of the pure spin current between our CFS/Cu and the other conventional F/N LSV devices. The plot of $\Delta R_S A$ versus d at RT for CFS/Cu LSVs and Py/Cu LSVs is shown in Fig. 3, together with

that at 80 K in the inset. The $\Delta R_S A$ is increased with decreasing d for both series of the CFS/Cu and Py/Cu LSV devices. By solving one dimensional spin diffusion equation[6, 23] (see Supplementary information), $\Delta R_S A$ can be expressed as

$$\Delta R_S A \approx \frac{\left(\frac{P_F}{(1-P_F^2)} \rho_F \lambda_F + \frac{P_I}{(1-P_I^2)} \text{RA}_{F/N} \right)^2}{\rho_N \lambda_N \sinh(d/\lambda_N)}, \quad (1)$$

where P_F and P_I are, respectively, the bulk and interface spin polarizations for F, λ_F and λ_N are the spin diffusion lengths for F and N, and, ρ_F and ρ_N are the resistivities for F and N, respectively. As shown in Fig. 3, the plots of $\Delta R_S A$ versus d for both series of the CFS/Cu and Py/Cu LSV devices are well reproduced by the fitting curves with $\lambda_{\text{Cu}} = 500$ nm and $\lambda_{\text{Cu}} = 1300$ nm at RT and 80 K[1, 2, 6, 7], respectively. For the Py/Cu LSVs, assuming $\lambda_{\text{Py,RT}} = 3$ nm and $\lambda_{\text{Py,80K}} = 5$ nm, we obtained a reasonable P_{Py} of 0.3 and 0.35 at RT and 80 K, respectively[1, 2, 6]. Thus, the above equation is a reliable for expressing the generation efficiency of the pure spin current among various LSVs. We then roughly estimate the spin polarization for CFS (P_{CFS}). Since it is impossible to determine the spin polarization and the spin diffusion length independently from the present results, we assume that λ_{CFS} is the same order of that for CFSA (see Supplementary information). If we use $\lambda_{\text{CFS,RT}} = 2 \sim 4$ nm and $\lambda_{\text{CFS,80K}} = 3 \sim 6$ nm, P_{CFS} can be estimated to be 0.56 ± 0.10 at RT and 0.67 ± 0.11 at 80 K, similar to the P estimated from the analysis of the current perpendicular GMR effects[24, 25]. Although the present CFS epitaxial layers have highly ordered structures with a high magnetic moment above $5 \mu_B/\text{f.u}$ [22], the value is still smaller than $6 \mu_B/\text{f.u}$. in the perfectly ordered CFS[19, 20]. Since further enhancement in P_{CFS} will be achieved by improving the crystal growth technique, a scaling characteristic with $P = 1$ will be obtainable ultimately (see dashed line). It should be noted that the resistivity for the ferromagnetic electrode (ρ_F) and the interface resistance area product ($\text{RA}_{F/N}$) are also important factors in Eq. (1). Therefore, the relatively large ρ_{CFS} and $\text{RA}_{\text{CFS/Cu}}$ compared to those in the Py/Cu LSV (see Method) are also advantages for obtaining large $\Delta R_S A$.

Our data for the CFS/Cu LSVs is approximately one hundred times as large as that for the Py/Cu LSV, indicating a significant improvement of the generation efficiency of the pure spin current using ohmic junctions. The present result is a markedly technological advance in spintronics using pure spin currents, generated by Heusler-compound spin injectors.

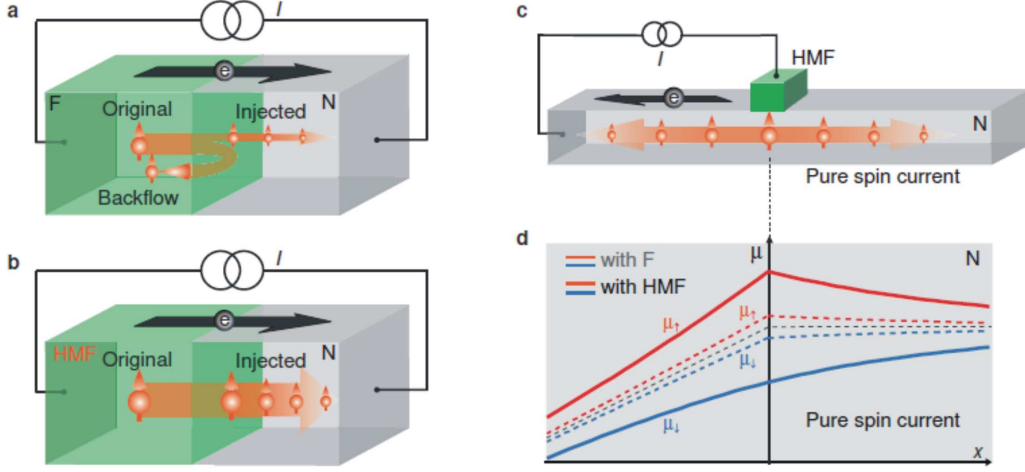


FIG. 1: **Concept of efficient generation of a pure spin current.** **a,b**, Schematic diagrams of the electrical spin injection from a conventional ferromagnet (F) or a half-metallic (HM) F into a nonmagnet (N). For the conventional F, most of the original spin currents go back to the F (a backflow of the spin current), giving rise to a significant reduction in the injected spin current. For the HMF, the original spin current is fully injected into the N without the backflow. **c**, Generation of a pure spin current by using nonlocal spin injection. The electron charges are extracted toward left hand side while the spin currents diffuse into both side symmetrically. **d**, Spatial distributions of the spin-dependent electro-chemical potentials, $(\mu_{\uparrow}, \mu_{\downarrow})$, in the N. Although the charge current $\propto \partial(\mu_{\uparrow} + \mu_{\downarrow})/\partial x$ is zero in the right hand side, a finite spin current $\propto \partial(\mu_{\uparrow} - \mu_{\downarrow})/\partial x$ is generated over the spin diffusion length. Thus, the pure spin current can be generated in the right hand side of the N.

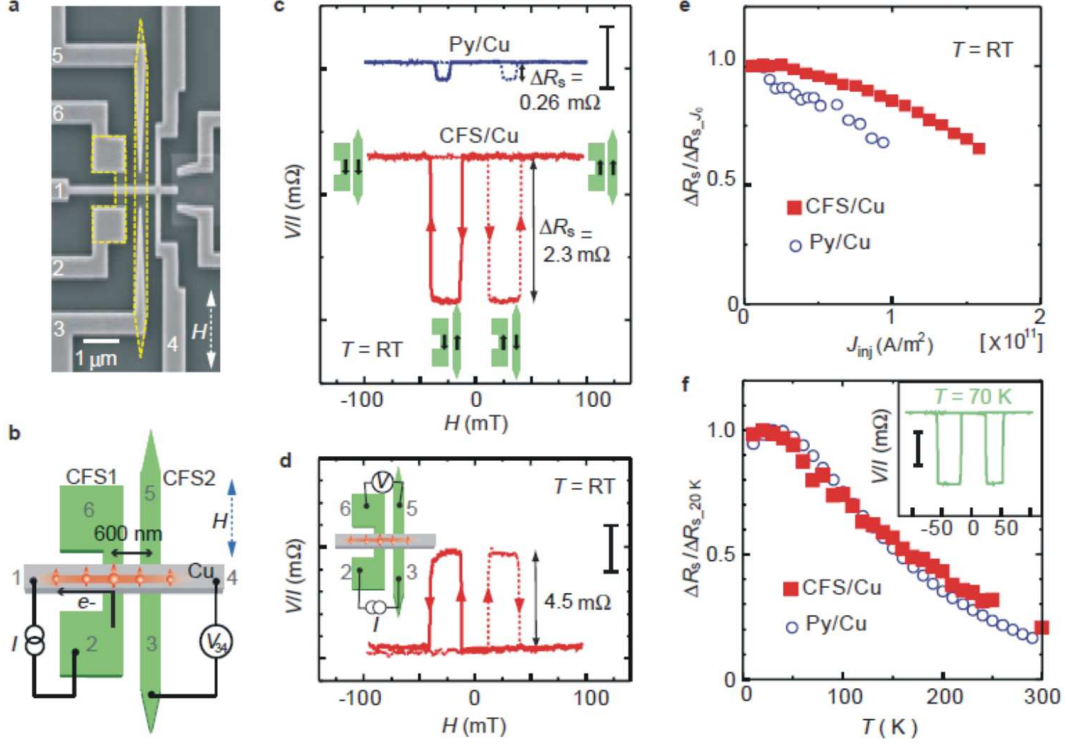


FIG. 2: **Giant nonlocal spin valve effect.** **a**, A scanning electron microscope image of the fabricated $\text{Co}_2\text{FeSi}(\text{CFS})/\text{Cu}$ lateral spin valve. **b**, Schematic of a nonlocal spin valve measurement. Spin-polarized electrons are injected from contact 2, and electron charges are extracted from contact 1. A nonlocal voltage is measured between contact 3 and contact 4. **c**, A room-temperature nonlocal spin-valve signal for the CFS/Cu LSV, together with that for the Py/Cu LSV. The signal varies according to the relative magnetization orientation of two wire-shaped CFS electrodes, as shown in the inset illustrations. **d**, A room-temperature local spin-valve signal for the CFS/Cu LSV. The inset shows the current-voltage probe configuration, i.e. the current is injected from contact 2 and extracted from contact 3, and the voltage is measured between contact 5 and contact 6. The low and high resistance states correspond to the parallel and anti-parallel magnetization alignments, respectively. The expected magnetization configurations agree with those observed in the nonlocal spin valve signal. **e**, Nonlocal spin signal ΔR_S as a function of J_{inj} at the injecting junction, normalized by ΔR_S at a small bias current density of $J_0 \sim 10^9 \text{ A/m}^2$, for the CFS/Cu LSV (red solid squares) and the Py/Cu LSV (blue open circles). **f**, Temperature dependence of ΔR_S for the CFS/Cu LSV (red solid squares) and the Py/Cu LSV (blue open circles), normalized by ΔR_S at 20 K. The inset shows a nonlocal spin-valve effect of the CFS/Cu LSV at $T = 70 \text{ K}$. The scale bars in c, d, and the inset of f are 1, 2, and 5 m Ω , respectively.

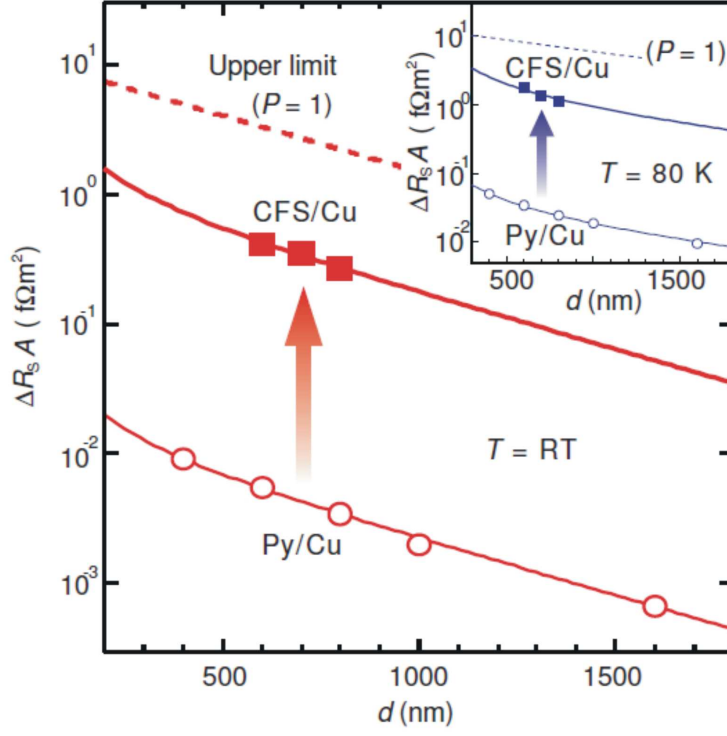


FIG. 3: **Scaling plot for lateral spin valve devices with metallic junctions.** The resistance change area product for the nonlocal spin signal ($\Delta R_S A$) as a function of d for CFS/Cu LSVs (filled squares), together with that for Py/Cu LSVs (open circles). The main panel and inset show the data at RT and 80 K, respectively. The solid curves are fitting results with $\lambda_{\text{Cu}} = 500$ nm at RT (red line) and $\lambda_{\text{Cu}} = 1300$ nm at 80 K (blue line), and the dashed curves are theoretical upper limits using $P = 1$, calculated from the equation, $\Delta R_S A = P^2 (S_{\text{Inj}} S_{\text{Det}} / S_N) \rho_{\text{Cu}} \lambda_{\text{Cu}} e^{-d/\lambda_{\text{Cu}}}$.

Method

As a spin injector- and detector-material, 25-nm-thick Co_2FeSi (CFS) films were grown on Si(111) templates by low temperature molecular beam epitaxy[22]. Prior to the growth, surface cleaning of substrates was performed with an aqueous HF solution (HF : H_2O = 1 : 40), and then, they were heat-treated at 450 °C for 20 min in an MBE chamber with a base pressure of 2×10^{-9} Torr. After the reduction in the substrate temperature down to 100 °C, we co-evaporated Co, Fe, and Si with stoichiometric chemical compositions by using Knudsen cells. During the growth, two-dimensional epitaxial growth was confirmed by observing reflection high energy electron diffraction patterns. The formed epitaxial CFS films were characterized by means of cross-sectional transmission electron microscopy (TEM), nanobeam electron diffraction (ED), and ^{57}Fe conversion electron Mössbauer spectroscopy. From these detailed characterizations, we have observed highly ordered $L2_1$ structures in the CFS layers[22]. Next, we patterned submicron-sized resist mask structures on the CFS films using a conventional electron-beam lithography. Then an Ar ion milling technique is employed to form the wire-shaped CFS spin injector and detector with 300 nm in width. One CFS wire is connected to two square pads to facilitate domain wall nucleation, while the other has pointed-end edges. Using the two different wire shapes, we can control the magnetization configuration by adjusting external magnetic fields (H), where H is applied along the CFS wires. Finally, top Cu strips, 200 nm in width and 100 nm in thickness, bridging the CFS wires and bonding pads were patterned by a conventional lift-off technique. Prior to the Cu deposition, the surfaces of the CFS wires were well cleaned by the Ar ion milling with a low accelerating voltage, resulting in low resistive ohmic interfaces with $R_{\text{CFS/Cu}} \approx 1 \text{ f}\Omega\text{m}^2$. Nonlocal and local spin valve measurements were carried out by a conventional current-bias lock-in technique (~ 200 Hz). The resistivities for the prepared CFS and Cu wires are $90.5 \mu\Omega\text{cm}$ and $2.5 \mu\Omega\text{cm}$ at RT and $54.6 \mu\Omega\text{cm}$ and $1.2 \mu\Omega\text{cm}$ at 80 K, respectively.

Acknowledgements

This work was supported by Fundamental Research Grants from CREST-JST and PRESTO-JST.

Author Information

T. K., N. H. and K. H. carried out the device fabrications and the transport measurements. S. Y., M. M. and K. H. prepared the epitaxial Co_2FeSi films. T. K. and K. H. performed the data analysis. T. K., M. M. and K. H. planned the present project and wrote the paper.

-
- [1] Jedema, J. F., Filip, T. A. & van Wees, J. B. Electrical spin injection and accumulation at room temperature in an all-metal mesoscopic spin valve. *Nature* **410**, 345-348 (2001).
- [2] Jedema, J. F., Nijboer, S. M., Filip, T. A. & van Wees, J. B. Spin injection and spin accumulation in all-metal mesoscopic spin valves. *Phys. Rev. B* **67**, 085319 (2003).
- [3] Chappert, C., Fert, A. & Frédéric Nguyen Van Dau. The emergence of spin electronics in data storage. *Nature Mater.* **6**, 813-823 (2007).
- [4] Žutić, I., Fabian, J. & Sarma, D. S. Spintronics: Fundamentals and applications. *Rev. Mod. Phys.* **76**, 323-410 (2004).
- [5] Uchida, K., Takahashi, S., Harii, K., Ieda, J., Koshibae, W., Ando, K., Maekawa, S. & Saitoh, E. Observation of the spin Seebeck effect. *Nature* **455**, 778-781 (2008).
- [6] Kimura, T., Hamrle, J. & Otani, Y. Estimation of spin-diffusion length from the magnitude of spin-current absorption: Multiterminal ferromagnetic/nonferromagnetic hybrid structures. *Phys. Rev. B* **72**, 014461 (2005).
- [7] Kimura, T., Otani, Y. & Hamrle, J. Enhancement of spin accumulation in a nonmagnetic layer by reducing junction size. *Phys. Rev. B* **73**, 132405 (2006).
- [8] Godfrey, R. & Johnson, M. Spin Injection in Mesoscopic Silver Wires: Experimental Test of Resistance Mismatch. *Phys. Rev. Lett.* **96**, 136601 (2006).
- [9] Yang, T., Kimura, T. & Otani, Y. Giant spin-accumulation signal and pure spin-current-induced reversible magnetization switching. *Nature Phys.* **4**, 851-854 (2008).
- [10] Kimura, T., Sato, T. & Otani, Y. Temperature evolution of spin relaxation in a NiFe/Cu lateral spin valve. *Phys. Rev. Lett.* **100**, 066602 (2007).
- [11] Valenzuela, O. S. & Tinkham, M. Spin-polarized tunneling in room-temperature mesoscopic spin valves. *Appl. Phys. Lett.* **85**, 5914-5916 (2004).
- [12] Kimura, T. & Otani, Y. Large spin accumulation in a permalloy-silver lateral spin valve. *Phys. Rev. Lett.* **99**, 196604 (2007).
- [13] Mihajlovic, G., Pearson E. J., Bader D. S. & Hoffmann A. Surface Spin Flip Probability of Mesoscopic Ag Wires. *Phys. Rev. Lett.* **104**, 237202 (2010)
- [14] Idzuchi, H., Fukuma, Y., Wang, L. & Otani, Y. Spin Diffusion Characteristics in Magnesium Nanowires. *Appl. Phys. Express* **3**, 063002 (2010).

- [15] Johnson, M. & Silsbee, R. H. Interfacial charge-spin coupling: Injection and detection of spin magnetization in metals. *Phys. Rev. Lett.* **55**, 1790-1793 (1985).
- [16] van Son, C. P., van Kempen, H. & Wyder, P. Boundary Resistance of the Ferromagnetic-Nonferromagnetic Metal Interface. *Phys. Rev. Lett.* **58**, 2271-2273 (1987).
- [17] Schmidt, G., Ferrand, D., Molenkamp, W. L. , Filip, T. A. & van Wees, J. B. Fundamental obstacle for electrical spin injection from a ferromagnetic metal into a diffusive semiconductor. *Phys. Rev. B* **62**, R4790-R4793 (2000).
- [18] de Groot, A. R., Mueller, M. F., van Engen, G. P. & Buschow, J. H. K. New Class of Materials: Half-Metallic Ferromagnets. *Phys. Rev. Lett.* **50**, 2024-2027 (1983).
- [19] Inomata, K., Ikeda, N., Tezuka, N., Goto, R., Sugimoto, S., Wojcik, M. & Jedryka, E. Highly spin-polarized materials and devices for spintronics. *Sci. Technol. Adv. Mater.* **9**, 014101 (2008).
- [20] Balke, B., Wurmehl, S., Fecher, H. G., Felser, C. & Kübler, J. Rational design of new materials for spintronics: Co_2FeZ ($Z = \text{Al, Ga, Si, Ge}$). *Sci. Technol. Adv. Mater.* **9**, 014102 (2008).
- [21] Sakuraba, Y., Hattori, M., Oogane, M., Ando, Y., Kato, H., Sakuma, A., Miyazaki, T. & Kubota, H. Giant tunneling magnetoresistance in $\text{Co}_2\text{MnSi}/\text{Al-O}/\text{Co}_2\text{MnSi}$ magnetic tunnel junctions. *Appl. Phys. Lett.* **88**, 192508 (2006).
- [22] Yamada, S., Hamaya, K., Yamamoto, K., Murakami, T., Mibu, K. & Miyao, M. Significant growth-temperature dependence of ferromagnetic properties for $\text{Co}_2\text{FeSi}/\text{Si}(111)$ prepared by low-temperature molecular beam epitaxy. *Appl. Phys. Lett.* **96**, 082511 (2010).
- [23] Takahashi, S. & Maekawa, S. Spin injection and detection in magnetic nanostructures. *Phys. Rev. B* **67**, 052409 (2003).
- [24] Nakatani, M. T., Furubayashi, T., Kasai, S., Sukegawa, H., Takahashi, K. Y., Mitani, S. & Hono, K. Bulk and interfacial scatterings in current-perpendicular-to-plane giant magnetoresistance with $\text{Co}_2\text{Fe}(\text{Al}_{0.5}\text{Si}_{0.5})$ Heusler alloy layers and Ag spacer. *Appl. Phys. Lett.* **96**, 212501 (2010).
- [25] Sakuraba, Y., Izumi, K., Iwase, T., Bosu, S., Saito, K., Takanashi, K., Miura, K., Futatsukawa, K., Abe, K., & Shirai, M. Mechanism of large magnetoresistance in $\text{Co}_2\text{MnSi}/\text{Ag}/\text{Co}_2\text{MnSi}$ devices with current perpendicular to the plane, *Phys. Rev. B* **82**, 094444 (2010).

Supplementary information

Introducing the resistance area product for nonlocal spin signals

In the lateral spin valve consisting of two ferromagnetic wire bridged by a nonmagnetic strip as shown in Figs. 2a and 2b, the nonlocal spin signal ΔR_S based on a one-dimensional spin diffusion model is given[1, 2] by

$$\Delta R_S = e^{-\frac{d}{\lambda_N}} \frac{R_{SN} \left(P_I \frac{R_{SI_{inj}}}{R_{SN}} + P_F \frac{R_{SF_{inj}}}{R_{SN}} \right) \left(P_I \frac{R_{SI_{det}}}{R_{SN}} + P_F \frac{R_{SF_{det}}}{R_{SN}} \right)}{\left(1 + 2 \frac{R_{SI_{inj}}}{R_{SN}} + 2 \frac{R_{SF_{inj}}}{R_{SN}} \right) \left(1 + 2 \frac{R_{SI_{det}}}{R_{SN}} + 2 \frac{R_{SF_{det}}}{R_{SN}} \right) - e^{-\frac{2d}{\lambda_N}}}. \quad (2)$$

Here P_F and P_I are the bulk and interface spin polarizations of the ferromagnetic electrode, respectively, and $R_{SF_{inj}}$, $R_{SF_{det}}$ and R_{SN} are the spin resistances for the ferromagnetic injector, detector and the nonmagnetic strip, respectively. Also, $R_{SI_{inj}}$ and $R_{SI_{det}}$ are the interface spin resistances for the injecting and detecting junctions. d and λ_N are the separation distance between the injector and detector and the spin diffusion length for the nonmagnetic strip. The spin resistance is defined as $2\rho\lambda/((1-P^2)S)$, where ρ , λ and S are the resistivity, the spin diffusion length and the effective cross section for the spin current, respectively. The interface spin resistance R_{SI} is defined by $2RA/((1-P_I^2)S)$, where RA is the resistance area product.

In the nonmagnetic strip with a long spin diffusion length over a few hundred nanometer, S is given by the cross section of the strip. On the other hand, in the ferromagnets with a short spin diffusion length less than 10 nm, S is given by the size of the junction in contact with the nonmagnetic strip because the spin current abruptly decays in the vicinity of the F/N interface[7]. Moreover, for the ohmic junction, the interface resistance is typically a few hundred mili ohm, which is also much smaller than R_{SN} . When $R_{SN} \gg R_{SF}, R_{SI}$, the above equation can be simplified as

$$\Delta R_S \approx \frac{(P_F R_{SF_{inj}} + P_I R_{SI_{inj}})(P_F R_{SF_{det}} + P_I R_{SI_{det}})}{2R_{SN} \sinh(d/\lambda_N)}. \quad (3)$$

It should be noted that although R_{SF} increases with P and diverges at $P = 1$, the condition of $R_{SF} \ll R_{SN}$ is still valid for $P < 0.9$ for the CFS film.

By introducing the junction sizes (S_{inj} , S_{det} and S_N), this equation can be revised as

$$\Delta R_S \approx \frac{S_N}{S_{inj} S_{det}} \frac{\left(\frac{P_F}{(1-P_F^2)} \rho_F \lambda_F + \frac{P_I}{(1-P_I^2)} RA_{F/N} \right)^2}{\rho_N \lambda_N \sinh(d/\lambda_N)}. \quad (4)$$

By defining $\Delta R_S A$ as $\Delta R_S(S_{\text{inj}}S_{\text{det}}/S_N)$, we obtain

$$\Delta R_S A \approx \frac{\left(\frac{P_F}{(1-P_F^2)} \rho_F \lambda_F + \frac{P_I}{(1-P_I^2)} R A_{F/N} \right)^2}{\rho_N \lambda_N \sinh(d/\lambda_N)}. \quad (5)$$

In Eq. (4), the influence of the junction sizes on the spin signal can be normalized. Thus, $\Delta R_S A$ allows us to fairly evaluate the generation efficiency of the pure spin current for various combinations of a ferromagnetic metal and a nonmagnetic one.

Estimation of interface resistance

The interface resistance was estimated by measuring the 4-terminal resistances with local spin valve configuration. In this configuration, the total resistance consists of the resistance of the Cu wire and the two interface resistances. Since the resistance of the Cu wire can be estimated from the resistivity for Cu, we can roughly calculate the interface resistance by subtracting the resistance for the Cu wire from that in the local spin valve configuration. By using the relation that the difference in the resistance ΔR is given by $R A_{F/N}(S_{\text{inj}} + S_{\text{det}})$, we can obtain $R A_{F/N}$. For the CFS/Cu LSVs, ΔR was $\sim 30 \text{ m}\Omega$, indicating $R A_{\text{CFS/Cu}} \sim 1 \text{ f}\Omega\text{m}^2$.

Estimation of spin polarization

By fitting the experimental data on the distance dependences of the $\Delta R_S A$ using Eq. (4), we can estimate the spin polarization of the spin injector in the LSV systems. For the Py/Cu LSVs, $R_{\text{Py/Cu}}$ is less than $0.1 \text{ f}\Omega\text{m}^2$, much smaller than $\rho_{\text{Py}} \lambda_{\text{Py}}$ ($0.75 \text{ f}\Omega\text{m}^2$). Thus, we can neglect the second term in the numerator of Eq. (3), then obtain $P_{\text{Py}} \sim 0.3$ at RT and 0.35 at 80 K , respectively with assuming $\lambda_{\text{Py,RT}} = 3 \text{ nm}$ and $\lambda_{\text{Py,80K}} = 5 \text{ nm}$ [3].

For the CFS/Cu LSVs, as described in the previous section, $R_{\text{CFS/Cu}}$ can be approximately estimated as $\sim 1 \text{ f}\Omega\text{m}^2$. Because of the following reasons, we assumed that the spin diffusion length for CFS (λ_{CFS}) is the same order of that for CFSA (λ_{CFSA}), which was reported as 2.2 nm at RT and 3 nm at 14 K in recent study of the vertical magnetoresistance device[6, 7]. The spin-diffusion length is proportional to the magnitude of the spin-orbit interactions. Since the atomic number of Al is close to Si, we expect that the magnitude of spin-orbit interaction in CFS should be almost same order of CFSA. From these considerations, we

expect that λ_{CFS} is the same level or shorter than λ_{CFSA} . Since the use of the longer λ_{CFS} prevents an overestimation of P_{CFS} , we use $\lambda_{\text{CFS,RT}} = 2 \sim 4$ nm and $\lambda_{\text{CFS,80K}} = 3 \sim 6$ nm, where the minimum value corresponds to λ_{CFSA} . We then obtained $P_{\text{CFS}} = 0.50 \sim 0.71$ at RT and $P_{\text{CFS}} = 0.66 \sim 0.81$ at 80 K with assuming $P_I = 0.5 \sim 0.7$, which is typical interface spin polarization between the Co-based alloy and Cu [4, 5].

Comparison of the device performance between LSVs with metallic and resistive interface resistances

In the present paper, we discuss the LSVs only with metallic junctions, since Eq. (1) is valid only for the condition of $\rho_F \lambda_F, \text{RA}_{\text{F/N}} \ll \rho_N \lambda_N$. When the above condition is not satisfied, for example, the LSVs with the resistive interface ($\text{RA}_{\text{F/N}} \gg \rho_N \lambda_N$) [8–10], the device performance cannot be evaluated by Eq (1). In order to fairly compare the device performance of different type LSVs, one should focus on the injection efficiency of the pure spin current. For the metallic junctions, the injection efficiency η_{I_S} of the pure spin current, which is defined by the ratio of the spin current I_S injected into the ferromagnetic contact to the excited charge current I_C , can be calculated as

$$\eta_{I_S} \equiv \frac{I_S}{I_C} \approx \frac{1}{2} \frac{S_N}{S_{\text{inj}}} \frac{\left(\frac{P_F}{(1-P_F^2)} \rho_F \lambda_F + \frac{P_I}{(1-P_I^2)} \text{RA}_{\text{F/N}} \right)}{\rho_N \lambda_N \sinh(d/\lambda_N)}. \quad (6)$$

For example, the injection efficiency of the present CFS/Cu LSV is estimated to be ~ 0.5 with $d = 100$ nm.

On the other hand, the efficiency for the LSV with the resistive interface, where $\text{RA}_{\text{F/N}} \gg \rho_N \lambda_N$, is given by

$$\eta_{I_S} \approx \frac{1}{4} P_I \frac{S_{\text{Det}}}{S_N} \frac{\rho_N \lambda_N}{\text{RA}_{\text{F/N}}} \exp^{-\frac{d}{\lambda_N}}. \quad (7)$$

In this case, the efficiency decreases with increasing the interface resistance area product $\text{RA}_{\text{F/N}}$. For example, for the Py/Ag LSVs with moderate interface resistances, where the large spin signals comparable to the present CFS/Cu LSV have been reported,[9, 10] the interface resistance area product $\text{RA}_{\text{F/N}}$ is 100 f Ωm^2 . Thus, the injection efficiency is estimated

to be ~ 0.005 with $d = 100$ nm.

-
- [1] Valet, T. & Fert, A. Theory of the perpendicular magnetoresistance in magnetic multilayers. *Phys. Rev. B* **48**, 7099-7113 (1993).
 - [2] Takahashi, S. & Maekawa, S. Spin injection and detection in magnetic nanostructures. *Phys. Rev. B* **67**, 052409 (2003).
 - [3] Kimura, T. & Otani, Y. Spin transport in lateral ferromagnetic/nonmagnetic hybrid structure. *J. Phys. Cond. Mat.* **19**, 165216 (2007).
 - [4] Vouille, C., Barthélémy, A., Elokani, M. F., Fert A., Schroeder, P. A., Hsu, S. Y., Reilly, A. & Loloee, R. Microscopic mechanisms of giant magnetoresistance. *Phys. Rev. B* **60**, 6710-6722 (1999).
 - [5] Baxter, J. R., Pettifor, G. D. & Tsymbal, Y. E. Interface proximity effects in current-perpendicular-to-plane magnetoresistance. *Phys. Rev. B* **71**, 024415 (2005).
 - [6] Nakatani, M. T., Furubayashi, T., Kasai, S., Sukegawa, H., Takahashi, Y. K., Mitani, S. & Hono K. Bulk and interfacial scatterings in current-perpendicular-to-plane giant magnetoresistance with $\text{Co}_2\text{Fe}(\text{Al}_{0.5}\text{Si}_{0.5})$ Heusler alloy layers and Ag spacer. *Appl. Phys. Lett.* **96**, 212501 (2010).
 - [7] Taniguchi T., Imamura H., Nakatani T., & Hono K., Effect of the number of layers on determination of spin asymmetries in current-perpendicular-to-plane giant magnetoresistance, *Appl. Phys. Lett.* **98**, 042503 (2011).
 - [8] Wang X. J., Zou H., Ocola L. E., and Ji Y. High spin injection polarization at an elevated dc bias in tunnel-junction-based lateral spin valves. *Appl. Phys. Lett.* **95**, 022519 (2009).
 - [9] Fukuma Y., Wang L., Idzuchi H. & Otani Y. Enhanced spin accumulation obtained by inserting low-resistance MgO interface in metallic lateral spin valves. *Appl. Phys. Lett.* **97**, 012507 (2010), Y. Fukuma, L. Wang, H. Idzuchi, S. Takahashi, S. Maekawa, and Y. Otani. Giant enhancement of spin accumulation and long-distance spin precession in metallic lateral spin valves. *Nature Mater.* **10**, 527 (2011)
 - [10] Mihajlovic G., Schreiber D. K. , Liu Y., Pearson J. E., Bader S. D. , Petford-Long A. K., & Hoffmann A. Enhanced spin signals due to native oxide formation in $\text{Ni}_{80}\text{Fe}_{20}/\text{Ag}$ lateral spin valves. *Appl. Phys. Lett.* **97**, 112502 (2010).